

1 **Generation of the internal pycnocline in the subpolar** 2 **Southern Ocean by wintertime sea ice melting**

3 **A. Klocker^{1,2*}, A. C. Naveira Garabato³, F. Roquet⁴, C. de Lavergne⁵, S. R.**
4 **Rintoul^{6,7,8}**

5 ¹Institute for Marine and Antarctic Studies, University of Tasmania, Hobart, Australia

6 ²Australian Research Council Centre of Excellence for Climate Extremes, University of Tasmania, Hobart,
7 Australia

8 ³Ocean and Earth Science, National Oceanography Centre, University of Southampton, Southampton,
9 United Kingdom

10 ⁴Department of Marine Sciences, University of Gothenburg, Gothenburg, Sweden

11 ⁵LOCEAN Laboratory, Sorbonne University-CNRS-IRD-MNHN, Paris, France

12 ⁶Commonwealth Scientific and Industrial Research Organisation, Environment, Hobart, Australia

13 ⁷Centre for Southern Hemisphere Oceans Research, CSIRO, Hobart, Australia

14 ⁸Australian Antarctic Program Partnership, University of Tasmania, Hobart, Australia

15 **Key Points:**

- 16 • The internal pycnocline in the high-latitude Southern Ocean is generated by winter-
17 persistent sea ice melting.
- 18 • Ice melt persists in winter due to ice drift and warm-water entrainment, maintain-
19 ing stratification at the base of the winter mixed layer.
- 20 • The subpolar internal pycnocline descends into the ocean interior at fronts of the
21 Antarctic Circumpolar Current.

*Current affiliation: NORCE Norwegian Research Centre, Bjerknnes Centre for Climate Research, Bergen,
Norway

Corresponding author: Andreas Klocker, ank1@norceresearch.no

Abstract

23 The ocean's internal pycnocline is a layer of elevated stratification that separates
24 the well-ventilated upper ocean from the more slowly-renewed deep ocean. Despite its
25 pivotal role in organizing ocean circulation, the processes governing the formation of the
26 internal pycnocline remain little understood. Classical theories on pycnocline formation
27 have been couched in terms of temperature and it is not clear how the theory applies in
28 the high-latitude Southern Ocean, where stratification is dominated by salinity. Here we
29 assess the mechanisms generating the internal pycnocline at southern high latitudes through
30 the analysis of a high-resolution, realistic, global sea ice–ocean model. We show evidence
31 suggesting that the internal pycnocline's formation is associated with sea ice-ocean in-
32 teractions in two distinct ice-covered regions, fringing the Antarctic continental slope and
33 the winter sea-ice edge. In both areas, winter-persistent sea-ice melt creates strong, salinity-
34 based stratification at the base of the winter mixed layer. The resulting sheets of high
35 stratification subsequently descend into the ocean interior at fronts of the Antarctic Cir-
36 cumpolar Current, and connect seamlessly to the internal pycnocline in areas further north
37 in which pycnocline stratification is determined by temperature. Our findings thus sug-
38 gest an important role of localized sea ice-ocean interactions in configuring the vertical
39 structure of the Southern Ocean.

Plain Language Summary

41 Satellite observations have revealed significant trends in Antarctic sea-ice concen-
42 tration over recent decades. While the science community is starting to unravel the causes
43 of the observed changes in sea-ice extent, our understanding of how these ice changes are
44 influencing ocean circulation remains rudimentary. Here we take a step toward address-
45 ing this important gap by analysing relationships between sea ice and ocean density struc-
46 ture in a state-of-the-art, realistic sea ice-ocean model. We find that localized sea ice-
47 ocean interactions in the Southern Ocean, in particular the counter-intuitive melting of
48 sea ice in winter, contribute to shape the vertical structure of the Southern Hemisphere
49 oceans.

50 1 Introduction

51 The internal pycnocline is a perennial layer of elevated density stratification, found
 52 at 200-1500 m over much of the ocean (Samelson & Vallis, 1997; Gnanadesikan, 1999).
 53 It is the main organizing feature of global ocean circulation, as it separates the relatively
 54 well-ventilated waters of the upper ocean, including those of the ventilated pycnocline
 55 (Luyten et al., 1983), from more slowly-renewed deeper waters (DeVries & Primeau, 2011).
 56 The abrupt vertical gradient in renewal time scale associated with the internal pycno-
 57 cline structures many important oceanic physical and chemical properties, such as salin-
 58 ity (Fig. 1b,d,f) or dissolved inorganic carbon (DeVries & Weber, 2017), thus fundamen-
 59 tally shaping the ocean’s climatic role (Khatiwala et al., 2012; DeVries & Holzer, 2019).

60 Classical views of the pycnocline – historically referred to as thermocline theory,
 61 since past work has focused on regions where stratification is set by temperature (often
 62 termed the *alpha ocean*, see (Carmack, 2007)) – propose two distinct mechanisms of py-
 63 cnocline formation. In adiabatic theories (Welander, 1959; Luyten et al., 1983; Huang,
 64 1988), the surface density distribution is set by atmospheric thermal forcing and trans-
 65 ferred to the ocean interior by wind-driven Ekman downwelling, which maps the surface
 66 meridional density gradient to a vertical profile. In contrast, diabatic theories (Robinson
 67 & Stommel, 1959; Stommel & Webster, 1962; Young & Ierley, 1986; Salmon, 1990) in-
 68 terpret the pycnocline as a diffusive front (or internal boundary layer) that forms at the
 69 convergence of warm near-surface waters and upwelling cold abyssal waters. In this view,
 70 the pycnocline thickness decreases as diabatic mixing weakens. Such adiabatic and di-
 71 abatic perspectives on pycnocline generation were subsequently unified in a two-regime
 72 model (Samelson & Vallis, 1997), according to which an upper, adiabatic part of the py-
 73 cnocline (the ventilated pycnocline) results from the vertical mapping of the surface merid-
 74 ional temperature gradient across the subtropical gyre; and a lower, diabatic part of the
 75 pycnocline (the internal pycnocline) is generated via a vertical advection - diffusion bal-
 76 ance, which recasts the surface meridional temperature difference across the subpolar
 77 gyre onto the vertical. This two-regime model, derived for a single-hemisphere closed basin,
 78 reproduces the main characteristics of the subtropical pycnocline and constitutes, to this
 79 day, the standard point of reference upon which our understanding of the pycnocline is
 80 based.

81 However, classical pycnocline theories may not directly address where or how ex-
 82 tensive parts of the internal pycnocline, such as that pervading the Southern Ocean, are
 83 formed. In much of that region, stratification is primarily determined by salinity (a regime
 84 often termed the *beta ocean* (Carmack, 2007)), with temperature having a destabilising
 85 effect on stratification. By focusing on temperature stratification, classical thermocline
 86 theories neglect potentially influential nonlinear interactions between temperature and
 87 salinity. Nonlinear interactions may arise in two main ways: (i) via the nonlinear depen-
 88 dence of density on temperature, salinity and pressure; and (ii) via the forcing of sur-
 89 face ocean temperature and salinity through distinct mechanisms with different spatio-
 90 temporal scales. Nowhere is the significance of such nonlinear interactions more evident
 91 than in the polar regions. There, the dominance of salinity in determining upper-ocean
 92 stratification maintains vast volumes of warm waters below the pycnocline and favours
 93 the wintertime formation of sea ice (Carmack, 2007) – the presence of which creates a
 94 powerful coupling between heat and freshwater fluxes (Martinson, 1990; Polyakov et al.,
 95 2017; Lecomte et al., 2017; Wilson et al., 2019). Recent work demonstrates the promi-
 96 nent global stratification impact of the nonlinear dependence of density on temperature
 97 and pressure (Nycander et al., 2015; Roquet et al., 2015), and highlights the large sen-
 98 sitivity of global stratification and sea-ice formation to seawater properties near the freez-
 99 ing point (Roquet et al., 2022).

100 In this paper, we show evidence from a realistic sea ice-ocean model which suggests
 101 that nonlinear interactions between temperature and salinity play an important role in
 102 the generation of the internal pycnocline in the subpolar Southern Ocean. Our illustra-
 103 tion of this result is framed in terms of potential vorticity (PV). Although vigorously mod-
 104 ified at the ocean boundaries, PV is approximately conserved in the ocean interior, where
 105 diabatic and frictional processes are generally modest (Vallis, 2006). Here, we define PV
 106 = $-\frac{f}{\rho} \frac{d\rho}{dz}$, where f is the Coriolis parameter, ρ is the surface-referenced potential den-
 107 sity, and $\frac{1}{\rho} \frac{d\rho}{dz}$ quantifies the vertical stretching of isopycnal layers. Relative vorticity is
 108 neglected in this definition, as it is small relative to planetary vorticity except in local-
 109 ized frontal regions (J. Marshall et al., 1993). Thus, PV is closely related to stratifica-
 110 tion, and the internal pycnocline is found to comprise several two-dimensional surfaces
 111 along which PV is elevated. We will refer to these two-dimensional surfaces as *high-PV*
 112 *sheets*.

113 2 Data and Methods

114 2.1 Global eddying sea ice-ocean model

115 Observations that resolve the seasonal cycle of surface forcing and hydrography in
 116 the Southern Ocean are presently scarce. We therefore turn to an eddying global sea ice-
 117 ocean simulation that has been thoroughly compared with observations and proven to
 118 be reasonably realistic (Kiss et al., 2020). The use of model output allows seasonally-
 119 varying surface fluxes to be linked to the seasonal evolution of stratification and PV. This
 120 enables us, in turn, to build an integrated picture of processes leading to the structure
 121 of the internal pycnocline.

122 The simulation uses a mesoscale eddy-rich version of the sea ice-ocean implemen-
 123 tation of the Australian Community Climate and Earth System Simulator, ACCESS-
 124 OM2, run at a horizontal resolution of 0.1° (ACCESS-OM2-01) with 75 vertical levels.
 125 The ocean model is MOM5.1 and the sea-ice model CICE5.1, coupled with the OASIS-
 126 MCT coupler. The model was forced with the JRA55-do v1.3 forcing data set. The ACCESS-
 127 OM2-01 experiment ran for 33 years from 1 January 1985 to 31 December 2017. It was
 128 started from a 40-year spin-up under repeated 1 May 1984 – 30 April 1985 JRA55-do
 129 forcing. Note that, while below we define the Stratification Control Index (SCI; see Ap-
 130 pendix B for further detail) in terms of conservative temperature Θ and absolute salin-
 131 ity S_A , the model uses potential temperature θ and practical salinity S_P instead. Hence,
 132 both PV and the SCI in the model are calculated using θ and S_P . Model fields are avail-
 133 able as monthly means. Details of the simulation and its evaluation can be found else-
 134 where (Kiss et al., 2020).

135 2.2 One-dimensional model of pycnocline generation

136 To understand the separate roles of temperature, salinity and wind forcing in the
 137 generation of the subpolar Southern Ocean pycnocline, we use the Massachusetts Insti-
 138 tute of Technology general circulation model (MITgcm (J. Marshall et al., 1997)) in a
 139 simple one-dimensional configuration with boundary conditions taken from the eddying
 140 global sea ice-ocean simulation. The 1-d model domain spans the uppermost 500 m of
 141 the water column, and has a vertical resolution of 1 m. Vertical mixing is parameterized
 142 using the K-profile parameterization (KPP (Large et al., 1994)). At the ocean surface
 143 and at 500 m, the 1-d model is restored to monthly-mean temperature and salinity val-

144 ues with a restoring time scale of one day, and a monthly-mean wind stress is applied
 145 at the surface. These values are taken from two locations in the global simulation ($70^{\circ}S, 100^{\circ}W$
 146 and $65^{\circ}S, 100^{\circ}W$), which are sited along the Pacific transect shown in Fig. 1c,d. The
 147 1-d model is initialised with conditions for December 2014, and cycled through one year
 148 of boundary conditions. The 1-d model simulations are spun up for 200 years, and the
 149 last 3 years are considered for analysis. In each of the two locations, we run (i) a sim-
 150 ulation with temperature/salinity/wind forcing, (ii) a simulation in which we exclude
 151 temperature forcing, (iii) a simulation in which we exclude salinity forcing, and (iv) a
 152 simulation without wind forcing. Intercomparison of these simulations enables us to high-
 153 light the crucial role of salinity forcing, set largely by sea ice-ocean interactions, in the
 154 generation of the local pycnocline.

155 **3 Results and Discussion**

156 **3.1 Relating potential vorticity to the Southern Hemisphere’s ocean struc-** 157 **ture**

158 The distribution of PV provides the organizing framework for the large-scale wa-
 159 ter mass structure and vertical circulation of the ocean. In the Southern Ocean and neigh-
 160 bouring Southern Hemisphere basins, this may be readily illustrated with meridional sec-
 161 tions of PV across the Indian, Pacific and Atlantic sectors (Fig. 1). PV exhibits a lay-
 162 ered arrangement, whereby thick layers of low PV are separated by thinner sheets of high
 163 PV. The thick, low-PV layers correspond to the major oceanic water masses, which fea-
 164 ture prominently in syntheses of the Southern Hemisphere ocean circulation (Talley, 2013;
 165 A. C. Naveira Garabato et al., 2014).

166 Specifically, the low-PV layers extending northward from the Southern Ocean in
 167 both the Indian and Pacific basins at depths of < 800 m contain Subantarctic Mode Wa-
 168 ter (SAMW; Fig. 1a-d). In the Atlantic basin, a low-PV layer residing at depths of < 500
 169 m encompasses Subtropical Mode Water (STMW; Fig. 1e-f). The low-PV layers extend-
 170 ing northward from the Southern Ocean in the Indian and Pacific basins (Atlantic basin)
 171 at depths of ~ 1000 m (~ 700 m) contain Antarctic Intermediate Water (AAIW). AAIW
 172 exhibits a broad sub-surface salinity minimum (Fig. 1b,d,f). Both STMW / SAMW and
 173 AAIW are characterized by relatively short ventilation time scales (McCartney, 1977;
 174 DeVries & Primeau, 2011). The deepest low-PV layer visible in Figure 1 encompasses

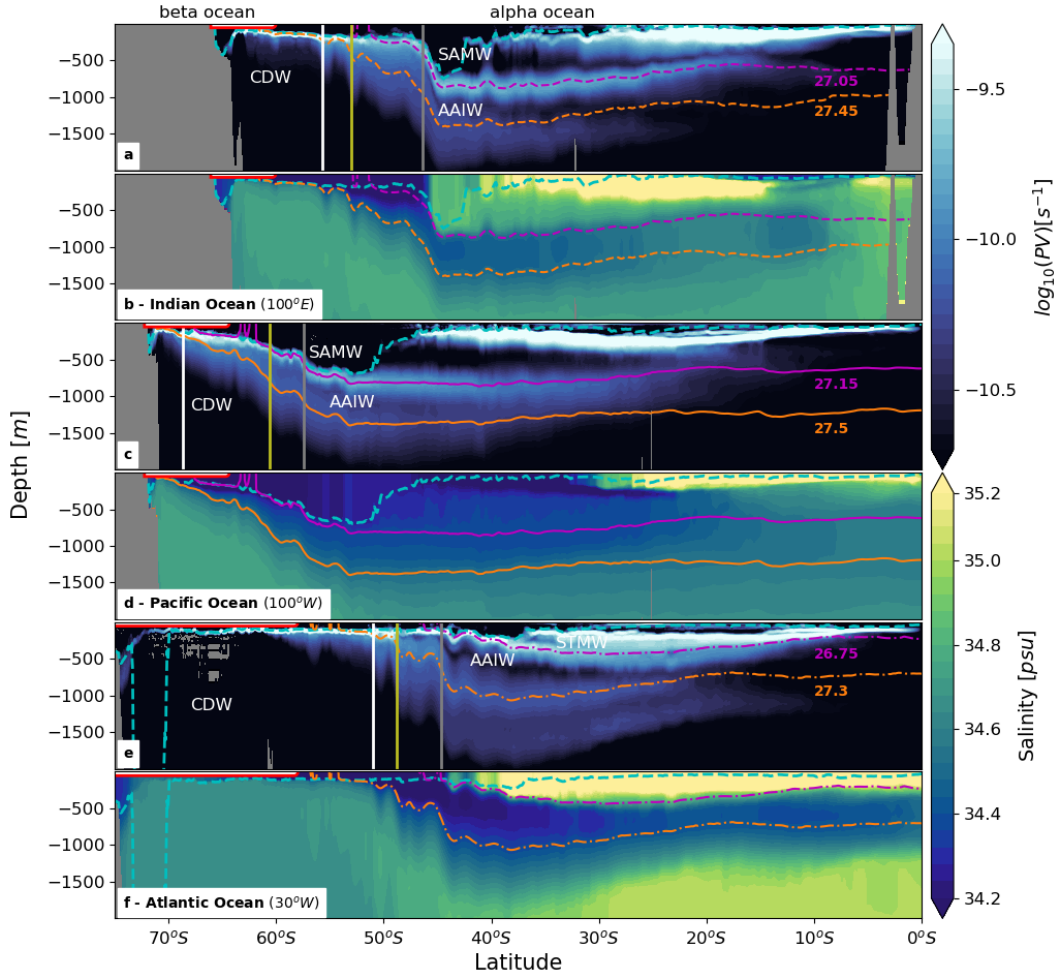


Figure 1. Potential vorticity and salinity. Winter values (shown for the month of September 2015) of (a,c,e) $\log_{10}(|PV|)$ and (b,d,f) salinity for a representative section in (a,b) the South Indian Ocean (100°E), (c,d) the South Pacific Ocean (100°W) and (e,f) the South Atlantic Ocean (30°W). Colored lines are isopycnal surfaces associated with the upper (magenta) and lower (orange) high-PV sheets, which together form the internal pycnocline

. Subantarctic Mode Water (SAMW), Antarctic Intermediate Water (AAIW), Circumpolar Deep Water (CDW) and Subtropical Mode Water (STMW) are labelled. The dashed cyan line represents the mixed layer depth. Vertical lines mark Southern Ocean fronts, in particular the Southern ACC front (SACCF; white), the Polar Front (PF; olive), and the Subantarctic Front (SAF; grey). Fronts are identified by maxima in isopycnal slopes and zonal flow, together with visual inspection of relevant hydrographic property gradients (Orsi et al., 1995). The red line at the surface shows the sea-ice extent, defined by sea-ice concentrations in excess of 15%. The beta ocean, in which stratification is determined by salinity, lies south of the PF. The alpha ocean, in which stratification is determined by temperature, lies north of the SAF.

175 Circumpolar Deep Water (CDW), a voluminous, slowly-renewed water mass that has sources
 176 in the North Atlantic and ultimately upwells in the Southern Ocean (Tamsitt et al., 2017).
 177 All of these water masses acquire their low PV at their surface formation sites, where
 178 intense wind and buoyancy forcings in winter trigger convective mixing and destroy strat-
 179 ification (Speer & Forget, 2001; Bullister et al., 2001).

180 In turn, the high-PV sheets bounding the low-PV layers define the fabric of the ocean’s
 181 pycnocline. The high-PV sheet closely following the 27.15 kg m^{-3} (27.05 kg m^{-3}) isopy-
 182 cnal in the Pacific (Indian) basin embodies the SAMW-AAIW interface. A less pronounced
 183 high-PV sheet is found at higher density, following the 27.5 kg m^{-3} (27.45 kg m^{-3}) isopy-
 184 cnal in the Pacific (Indian) Ocean, and constitutes the AAIW-CDW interface. A sim-
 185 ilar framework of two high-PV sheets exists in the Atlantic basin, where the sheets fol-
 186 low lighter isopycnals than in the Indo-Pacific sector and act as the STMW-AAIW and
 187 AAIW-CDW interfaces.

188 Jointly, the two high-PV sheets in the Pacific and Indian basins, at the upper and
 189 lower boundaries of AAIW, give rise to the stratification maximum that defines the in-
 190 ternal pycnocline (In Fig. 1(a-d), the internal pycnocline is the region of elevated PV be-
 191 tween the magenta and orange density contours.) In the Atlantic basin, the internal py-
 192 cnocline integrates only the denser high-PV sheet (the lighter sheet is embedded within
 193 the subtropical gyre’s base, and thereby contributes to the ventilated pycnocline). In all
 194 basins, the internal pycnocline extends seamlessly from mid latitudes, across the South-
 195 ern Ocean, to the Antarctic margins. The simulated pycnocline structure resembles that
 196 identified in hydrographic observations (Fig. A1; Appendix A), although the observations
 197 display a more subtle inter-sheet separation concealed by finescale processes (such as in-
 198 ternal waves) absent from the model, and slight differences in the density of the high-
 199 PV sheets. A possible factor underpinning the model-observations differences is the model’s
 200 use of zero explicit background vertical diffusion. Although this is unlikely the most re-
 201 alistic choice, zero background diffusion facilitates the tracing of the Southern Ocean py-
 202 cnocline’s PV signature to its generation regions, and thereby results in a clearer view
 203 of the generation mechanism.

204 The anatomy of the high-PV sheets forming the internal pycnocline offers several
 205 important hints as to the pycnocline’s origin (Fig. 1a,c,e). As one traces the high-PV sheets
 206 southward, approximately following isopycnals, their PV increases as the sheets draw near

207 the surface in the seasonally ice-covered Southern Ocean. There, the high-PV sheets de-
 208 viate significantly from density surfaces, as would be expected if diabatic or frictional
 209 processes were modifying PV locally. Thus, the structure of the high-PV sheets mak-
 210 ing up the Southern Hemisphere’s internal pycnocline suggests that the elevated strat-
 211 ification is generated in the upper layers of the seasonally ice-covered Southern Ocean.
 212 The generation mechanism of the high-PV sheets is assessed next.

213 **3.2 High-PV generation in the ice-covered Southern Ocean**

214 The generation of high PV in the ice-covered Southern Ocean may be understood
 215 in terms of two factors. First, the high-PV sheets originate near the surface in areas where
 216 salinity overwhelms temperature in determining stratification. This indicates that sur-
 217 face freshwater forcing is likely to play a central role in the creation of the high-PV sheets.
 218 Second, in order for these sheets to establish the internal pycnocline, their stratification
 219 must survive PV destruction by surface buoyancy loss and vertical mixing in winter.

220 To further unravel these factors, the seasonal evolution of upper-ocean PV and salin-
 221 ity along a representative meridional section at 100°W, in the Pacific basin, is shown in
 222 Fig. 2. Panels in each column correspond to every third month of the year, starting in
 223 December. Colored contours denote density surfaces of particular significance to the py-
 224 cnocline’s structure, as highlighted in Fig. 1. The dashed cyan line marks the mixed layer
 225 base. The bottom panels provide the equivalent sections of potential temperature (Fig. 2i)
 226 and the SCI (Fig. 2j) in winter (shown for the month of September). The SCI is an in-
 227 dex that indicates the relative contributions of temperature and salinity to setting the
 228 stratification, or PV. By construction, the SCI has three distinct regimes: $SCI < -1$ cor-
 229 responds to a stable stratification controlled by salinity where the thermal stratification
 230 is unstable (as often found in polar regions); $-1 < SCI < 1$ is associated with thermal
 231 and haline stratification that are both stable; and $SCI > 1$ is obtained when temper-
 232 ature controls the density stratification in the presence of a destabilizing effect of salin-
 233 ity. See Appendix B for a more lengthy explanation of the SCI, and how it relates to other
 234 stratification indicators more commonly used in the literature.

235 The highest PV values occur at the base of the buoyant mixed layer at the end of
 236 summer (Fig. 2c), when inputs of ice melt, meteoric freshwater and heat create fresh and
 237 light Antarctic Surface Water (Fig. 2d). The summer mixed layer base marks the loca-

238 tion of the seasonal pycnocline (Carmack, 2007; Pellichero et al., 2017). As the atmo-
 239 sphere cools and sea ice (shown by orange bars) rapidly expands in autumn, heat loss
 240 and brine rejection deepen the mixed layer and progressively erode the seasonal pycn-
 241 ocline (Fig. 2e,f). The upper-ocean density increase and mixed layer deepening continue
 242 over winter (Fig. 2g,h). Yet, despite the strong surface buoyancy loss and vertical mix-
 243 ing in autumn and winter, two distinct regions withstand the destruction of high PV at
 244 the base of the mixed layer. The 69-72°S latitude band holds the key to the generation
 245 and preservation of high PV along the 27.5 kg m^{-3} isopycnal (i.e. the denser of the high-
 246 PV sheets making up the internal pycnocline), which reaches its shallowest point and
 247 highest PV there. The 63-69°S latitude band hosts the formation of the lighter (27.15
 248 kg m^{-3}) of the high-PV sheets, which attains its maximum PV in the area. Both of these
 249 high-PV source regions are characterized by a $\text{SCI} < -1$ (Fig. 2j): cold near-surface wa-
 250 ters overlie warmer deeper waters in winter, and salinity determines upper-ocean strati-
 251 fication (Fig. 2i).

252 The preferential imprinting of high PV on shallow isopycnals in the two highlighted
 253 regions invites us to ask the question of what sets these areas apart. A first step toward
 254 an answer is provided by examination of the sea ice-ocean freshwater flux (Fig. 3e; the
 255 total surface freshwater flux, including surface restoring terms, is shown in Fig. C1 and
 256 discussed in Appendix C). Both high-PV generation regions host net sea-ice melt in win-
 257 ter. This counter-intuitive result has a different physical explanation in the southern and
 258 northern regions. In the southern area (69-72°S), net sea-ice melt is related to upwelling
 259 of warm CDW (Wilson et al., 2019), which is shallowest in this region (Fig. 2i). Once
 260 the seasonal pycnocline has been eliminated in the autumn, sea-ice formation leads to
 261 entrainment of warm CDW into the surface mixed layer. The entrained heat melts the
 262 existing sea ice and hinders further ice formation (Libera et al., 2022). This well-documented
 263 negative feedback on sea-ice formation (Martinson, 1990; Wilson et al., 2019) maintains
 264 the low salinity of the mixed layer. As a result, the strong, salinity-determined strati-
 265 fication (i.e. high PV) at the mixed layer base is preserved through winter (Fig. 2g,j) against
 266 the upwelling of CDW (Evans et al., 2018). Thus, the isopycnal lying at the mixed layer
 267 base in the area (27.5 kg m^{-3}) is imprinted with high PV.

268 In contrast, north of 69°S in Fig. 2, the sub-surface heat reservoir of CDW lies con-
 269 siderably deeper (Fig. 2i) and no longer provides a leading-order feedback on the win-
 270 tertime evolution of sea ice (Wilson et al., 2019). In this area, high-PV values below the

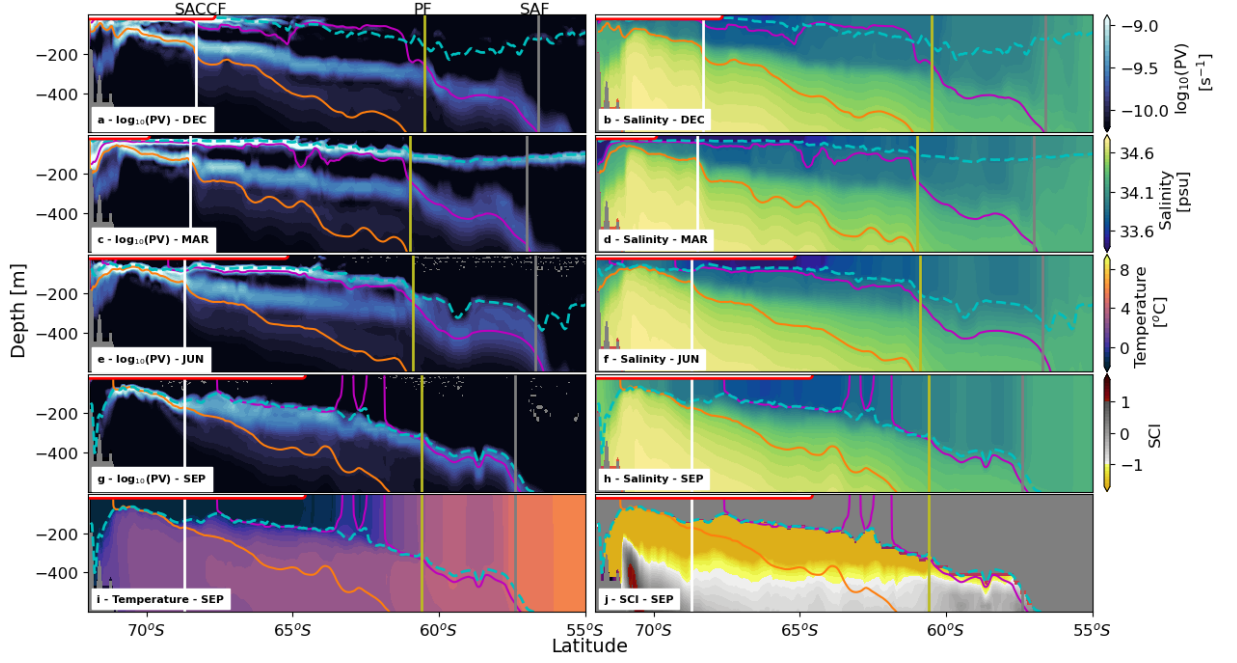


Figure 2. Seasonal evolution of potential vorticity and salinity in the Pacific sector. A latitude-depth section at 100°W of (a,c,e,g) $\log_{10}(|PV|)$ and (b,d,f,h) salinity for (a,b) December, (c,d) March, (e,f) June, and (g,h) September of year 2014/2015. (i) Temperature, and (j) Stratification Control Index SCI at 100°W for June 2015. Colored lines are isopycnal surfaces $\sigma_{\Theta} = 27.15 \text{ kg m}^{-3}$ (magenta) and 27.5 kg m^{-3} (orange). Dashed cyan line shows the mixed layer depth. Vertical lines mark Southern Ocean fronts, in particular, the Southern ACC front (SACCF; white), the Polar Front (PF; olive) and the Subantarctic Front (SAF; grey). Fronts are identified by maxima in isopycnal slopes and zonal flow, together with visual inspection of relevant hydrographic property gradients (Orsi et al., 1995). Red line at the surface indicates the sea-ice extent, defined by sea-ice concentrations in excess of 15%.

271 mixed layer are maintained by the continuous influx of sea ice, which drifts from the main
 272 freezing sites near the Antarctic margins toward the open ocean (Haumann et al., 2016).
 273 The import of sea ice impedes wintertime PV destruction through two effects. First, the
 274 sea-ice cover acts as a thermodynamic and mechanical insulator that dampens oceanic
 275 heat loss and wind-driven mechanical mixing (Sturm & Massom, 2009; Thorndike & Colony,
 276 1982), and thus suppresses the erosion of upper-ocean stratification. Second, near and
 277 to the north of the winter sea-ice edge, near-surface waters remain sufficiently warm year-
 278 round to melt sea ice drifting into the region (Fig. 3b). Because of these two factors, sea-
 279 ice melting prevails over much of the open Southern Ocean – including in winter (Fig. 3e)
 280 – and the seasonal densification of the mixed layer is limited (Fig. 2d-h). Hence, like in
 281 the southern high-PV source region, the surface mixed layer in this area remains very
 282 fresh in winter (Fig. 2h), despite forcing by the cold and windy atmosphere and by dif-
 283 fusive salt gain from the underlying CDW. Elevated, salinity-determined stratification
 284 is then maintained year-round on the isopycnal lying at the base of the winter mixed layer
 285 (27.15 kg m^{-3}) in the area straddling the late winter sea-ice edge, and the internal py-
 286 cnocline’s lighter high-PV sheet is formed.

287 To more quantitatively elicit the separate roles of temperature, salinity and wind
 288 forcing on the generation of the subpolar Southern Ocean pycnocline, we now turn to
 289 the one-dimensional model for the upper water column introduced in section 2.2. These
 290 one-dimensional simulations are run for two locations along the $100^\circ W$ Pacific section,
 291 at $70^\circ S$ and $65^\circ S$. The temperature and salinity at the surface and at 500 m are restored
 292 to values from the global simulations, and the wind forcing is taken from the global model
 293 as well. A resulting 3-year time series of $\log_{10}(|PV|)$, shown in Fig. 4a,b, approximately
 294 reproduces the pycnocline’s seasonal evolution in the realistic global model. For each of
 295 the two Pacific sector locations, we next run three additional 1-d simulations in which
 296 we exclude either temperature, salinity or wind forcing at the surface. If we exclude tem-
 297 perature forcing (Fig. 4c,d), the ensuing pycnocline is very similar to that in the simu-
 298 lation with full forcing, with PV values slightly smaller. If we exclude salinity forcing
 299 (Fig. 4e,f), the pycnocline vanishes and full-depth mixing occurs. If we exclude wind forc-
 300 ing (Fig. 4g,h), the internal pycnocline is slightly shallower, but still very similar, to that
 301 in the simulation with full forcing. These results thus show that it is surface freshwa-
 302 ter forcing that is key to generating the internal pycnocline at these locations. Given that
 303 almost all surface freshwater forcing in the seasonally ice-covered Southern Ocean is as-

sociated with sea ice-ocean interactions (Appendix C, Fig. C1), it is evident that only such interactions can generate the internal pycnocline in the beta ocean regime of the Southern Ocean.

To the north of their formation sites, the internal pycnocline's two high-PV sheets descend into the ocean interior along isopycnals at distinct locations (Fig. 2). These locations correspond with specific fronts of the Antarctic Circumpolar Current (ACC) (Orsi et al., 1995), where (sub-)mesoscale processes linked to the fronts' enhanced horizontal density gradients and vertical shears have been shown to induce along-isopycnal subduction of near-surface waters (A. Naveira Garabato et al., 2001; Klocker, 2018; Bachman & Klocker, 2020). Examination of Fig. 2 indicates that the deeper of the high-PV sheets, extending along the 27.5 kg m^{-3} isopycnal in the Pacific basin, departs from the winter mixed layer base and dives into the interior at the Southern ACC Front (SACCF). Similarly, the shallower of the high-PV sheets, found at the 27.15 kg m^{-3} isopycnal in the Pacific sector, descends into the interior at the Polar Front (PF). These qualitative relationships between the spatial configuration of high-PV sheets and the ACC's frontal structure are reproduced all around the Southern Ocean (Figs. 2, 5 and 6), and point to the existence of a dynamical underpinning of the sheets' downward and northward continuation from their subpolar generation areas. While the precise nature of these dynamics cannot be ascertained with the model data available, we hypothesize that the descent of the high-PV sheets into the interior is controlled by the same processes that govern frontal subduction (A. Naveira Garabato et al., 2001). Establishing whether this control is exerted directly via the northward transport of elevated PV along the pycnocline's isopycnals, or indirectly via the absence of low-PV injection on those isopycnals, will be the subject of a follow-up study.

3.3 Circumpolar view of internal pycnocline generation

The processes generating the internal pycnocline in the Pacific sector (Fig. 2) are widely generic around the Southern Ocean. To illustrate this point, Figures 3 a-d compare the horizontal distributions of wintertime (shown for the month of September) upper-ocean PV, thermohaline properties and SCI at an illustrative depth of 89 m, which is close to the base of the winter mixed layer south of the PF (Fig. 2). The wintertime surface freshwater flux due to the melting and freezing of sea ice is also shown in Fig. 3e.

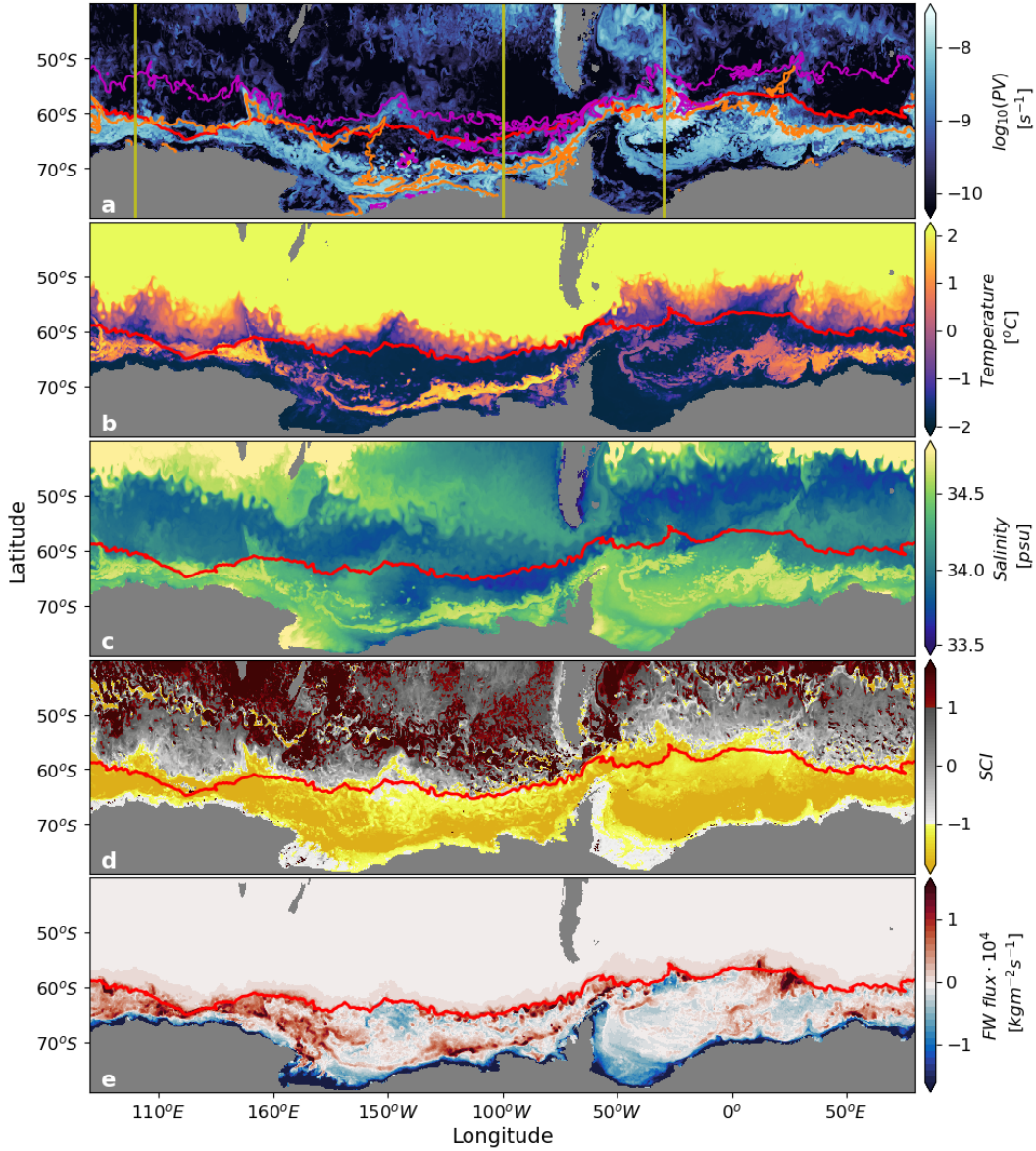


Figure 3. Circumpolar view of pycnocline formation in the upper ocean. (a) $\log_{10}(|PV|)$, (b) temperature, (c) salinity, and (d) Stratification Control Index SCI , at a depth of 89 m in September 2015. (e) Wintertime (July to September 2015) mean of surface freshwater flux due to sea-ice melting and freezing. Positive fluxes are directed into the ocean (melting ice). Magenta and orange contours in panel a respectively indicate isopycnal surfaces $\sigma_{\Theta} = 27.15 \text{ kg m}^{-3}$ and $\sigma_{\Theta} = 27.5 \text{ kg m}^{-3}$. The red line at the surface shows the sea-ice extent, defined as the northern terminus of sea-ice concentrations in excess of 15%. Olive lines in (a) show the location of the vertical sections shown in Figures

2, 5, and 6.

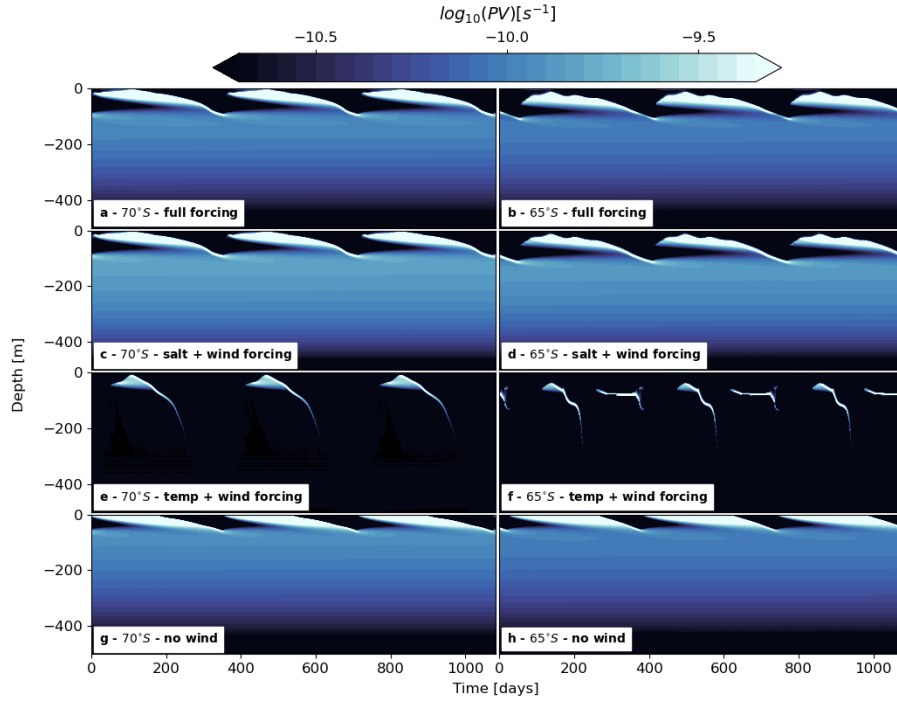


Figure 4. One-dimensional model of pycnocline generation. The evolution of $\log_{10}(|PV|)$ in the one-dimensional model is shown for 3 years, with forcing repeating annually and starting in December 2014, for two Pacific sector locations, **(a,c,e,g)** $70^\circ S, 100^\circ W$ and **(b,d,f,h)** $65^\circ S, 100^\circ W$. The simulations are run with **(a,b)** the full temperature/salinity/wind forcing, **(c,d)** salinity and wind forcing, **(e,f)** temperature and wind forcing, and **(g,h)** temperature and salinity forcing.

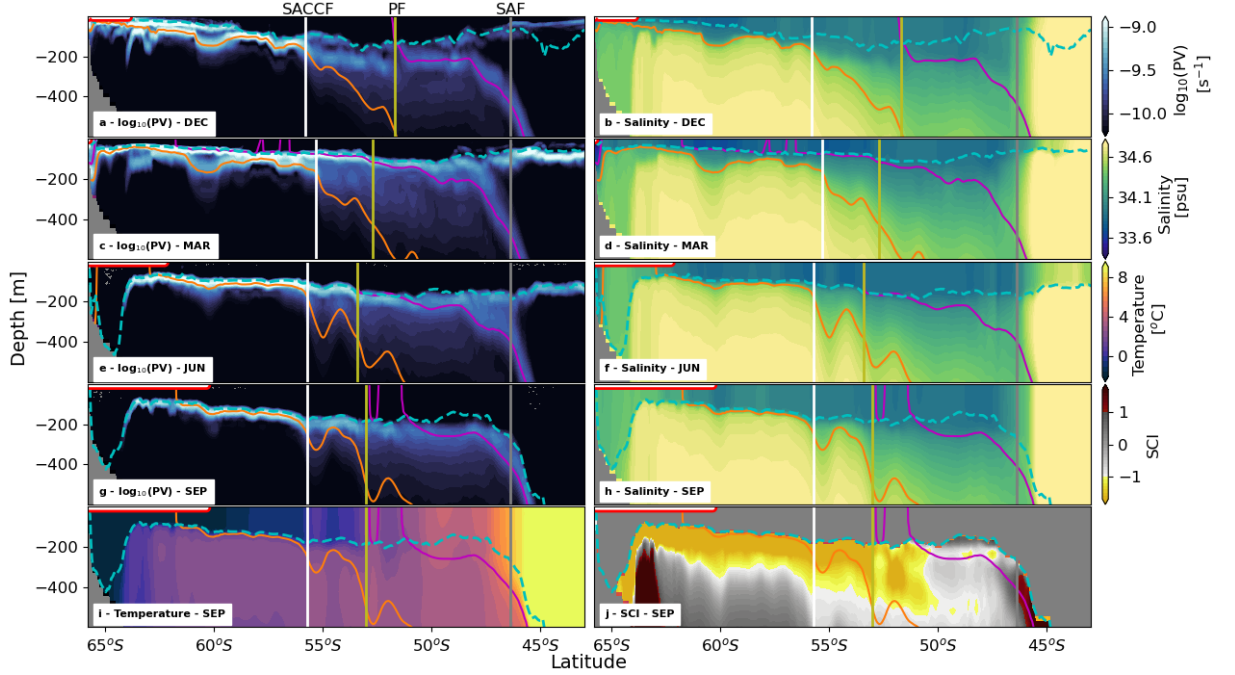


Figure 5. Seasonal evolution of potential vorticity and salinity in the Indian sector. A latitude-depth section at 100°E of (a,c,e,g) $\log_{10}(|PV|)$ and (b,d,f,h) salinity for (a,b) December, (c,d) March, (e,f) June, and (g,h) September of year 2014/2015. (i) Temperature, and (j) *SCI* at 100°E for September 2015. Colored dashed lines are isopycnal surfaces $\sigma_{\Theta} = 27.05 \text{ kg m}^{-3}$ (magenta) and 27.5 kg m^{-3} (orange). Dashed cyan line shows the mixed layer depth. Vertical lines mark Southern Ocean fronts, in particular the Southern ACC front (SACCF; white), the Polar Front (PF; olive), and the Subantarctic Front (SAF; grey). Fronts are identified by maxima in isopycnal slopes and zonal flow, together with visual inspection of relevant hydrographic property gradients (Orsi et al., 1995). Red line at the surface indicates the sea-ice extent, defined by sea-ice concentrations in excess of 15%.

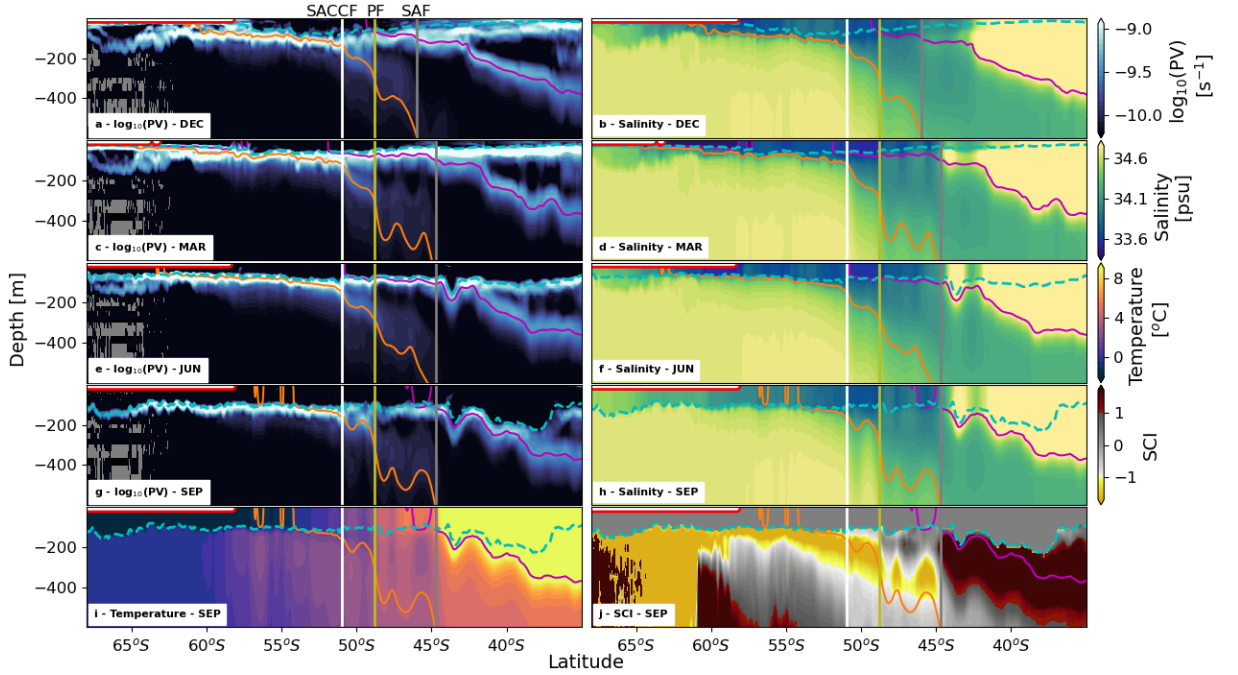


Figure 6. Seasonal evolution of potential vorticity and salinity in the Atlantic sector. A latitude-depth section at 30°W of (a,c,e,g) $\log_{10}(|PV|)$ and (b,d,f,h) salinity for (a,b) December, (c,d) March, (e,f) June, and (g,h) September of year 2014/2015. (i) Temperature, and (j) *SCI* at 30°W for September 2015. Colored dash-dotted lines are isopycnal surfaces $\sigma_{\Theta} = 27.15 \text{ kg m}^{-3}$ (magenta) and 27.5 kg m^{-3} (orange). Dashed cyan line shows the mixed layer depth. Vertical lines mark Southern Ocean fronts, in particular the Southern ACC front (SACCF; white), the Polar Front (PF; olive), and the Subantarctic Front (SAF; grey). Fronts are identified by maxima in isopycnal slopes and zonal flow, together with visual inspection of relevant hydrographic property gradients (Orsi et al., 1995). Red line at the surface indicates the sea-ice extent, defined by sea-ice concentrations in excess of 15%.

335 Wintertime upper-ocean PV is elevated along a several hundred kilometre-wide,
 336 circumpolar swath immediately to the north of the Antarctic continental shelf break (light
 337 blue shading in Fig. 3 a). This swath delineates the generation area of the denser high-
 338 PV sheet, as can be gleaned from the approximate spatial correspondence between the
 339 band of increased PV and the 27.5 kg m^{-3} isopycnal (orange contour in Fig. 3 a), on which
 340 that high-PV sheet lies in the Pacific basin. The lighter high-PV sheet, formed further
 341 to the north, is not visible in this map because the mixed layer is deeper further north,
 342 hence the lighter PV sheet is generated at a greater depth (see the high-PV sheet on the
 343 green isopycnal in Fig. 2g). The swath of elevated PV encircling Antarctica coincides with
 344 an area of higher temperature (Fig. 3b) and salinity (Fig. 3c), and reduced SCI (SCI <
 345 -1 , yellow shading in Fig. 3d). These indicate the shoaling of relatively warm and saline
 346 CDW beneath cold and fresh near-surface waters, which gives rise to strong, salinity-determined
 347 upper-ocean stratification. The association of high-PV generation, CDW shoaling and
 348 elevated salinity-induced stratification with the ice-ocean feedback outlined above (Martinson,
 349 1990; Wilson et al., 2019) is supported by the horizontal distribution of the surface fresh-
 350 water flux due to the melting and freezing of sea ice (Fig. 3e): the swath of high PV is
 351 broadly aligned with a band of substantial freshwater input to the ocean (red shading)
 352 fringing the Antarctic continental shelf break.

353 A second region of enhanced surface freshwater input occurs further to the north,
 354 around the winter sea-ice edge (Fig. 3e), and is linked to the generation of the lighter high-
 355 PV sheet. The excess freshwater forcing in this area produces an abrupt northward re-
 356 duction in mixed layer salinity (Fig. 3c), and is associated with a meridional transition
 357 from near-freezing to above-zero mixed layer temperature (Fig. 3b). Such thermohaline
 358 signatures suggest that the reduction in salinity stems at least in part from the melting
 359 of sea ice transported into warmer surface waters via wind-driven, northward Ekman drift
 360 (Haumann et al., 2016). More generally, persistent surface freshwater gain in this cir-
 361 cumpolar band of reduced surface salinity enables the preservation of elevated PV at the
 362 winter mixed layer base on the isopycnal coincident with the lighter high-PV sheet.

363 Although the key pycnocline formation features highlighted above are quasi-circumpolar,
 364 some differences between distinct sectors of the Southern Ocean are also apparent (cf.
 365 Figs. 2, 5 and 6). Most notably, the South Atlantic internal pycnocline incorporates one
 366 high-PV sheet only, at a considerably lighter isopycnal than the denser high-PV sheets
 367 in the Indo-Pacific sector. This is because, upon entering the South Atlantic, the ACC

368 veers sharply northward, leading to a significant rearrangement of ACC frontal locations
369 and surface buoyancy flux patterns. As a result, unlike in the other basins, the SACCF
370 in the South Atlantic lies consistently to the north of the winter sea-ice edge, such that
371 all melt-generated, high-PV waters at the winter mixed layer base within this sector are
372 collated into a single sheet descending into the interior at the SACCF (Fig. 6).

373 4 Conclusions and Outlook

374 Our analysis of a realistic sea ice–ocean model suggests that the internal pycno-
375 cline of the high-latitude Southern Ocean is generated by forcing and processes that are
376 distinct from those highlighted by classical views of pycnocline formation (Welander, 1959;
377 Luyten et al., 1983; Huang, 1988; Robinson & Stommel, 1959; Stommel & Webster, 1962;
378 Young & Ierley, 1986; Salmon, 1990), in the following ways.

379 First, the high stratification defining the internal pycnocline in this region is de-
380 termined by salinity, whereas classical theories of pycnocline generation focus on oceanic
381 regions with temperature-determined stratification. The stratification control by salin-
382 ity is primarily a result of the reduced thermal expansion coefficient near the freezing
383 point (Roquet et al., 2022). The key external forcing driving the formation of the region’s
384 internal pycnocline is freshwater input by sea-ice melt in winter (Fig. 3e). The melting
385 is localized to two distinct zones: one offshore of the Antarctic continental shelf break,
386 where sea-ice melt is sustained by the upward entrainment of warm CDW (Martinson,
387 1990; Wilson et al., 2019), and another fringing the winter sea-ice edge, where sea ice
388 melts as it drifts northward into warmer surface waters (Haumann et al., 2016). These
389 two wintertime melting zones give rise to two sheets of high stratification, and confer the
390 simulated internal pycnocline with a double stratification-maximum structure (Fig. 1).
391 This highlights how the strong coupling between thermal and freshwater forcings asso-
392 ciated with sea-ice formation and melt acts to configure ocean stratification on basin scales.

393 Second, the production of high stratification within the region’s internal pycnocline
394 does not stem from the downward projection of a meridional surface density gradient along
395 outcropping isopycnals, as in classical theories (Luyten et al., 1983; Samelson & Vallis,
396 1997), but rather from the production of a vertical density gradient at the base of the
397 winter mixed layer. Thus, the density classes hosting the internal pycnocline across and
398 beyond the high-latitude Southern Ocean need not reach the surface to acquire their el-

399 elevated stratification. This implies that the internal pycnocline’s density structure may
400 be controlled by sub-surface mixing processes around the mixed layer base, rather than
401 directly by buoyancy fluxes across the ocean surface.

402 Third, our finding that the descent of the high-PV sheets into the ocean interior
403 is localized to specific ACC fronts suggests that (sub-)mesoscale upper-ocean frontal dy-
404 namics may shape this stage of pycnocline formation. This contrasts with classical views,
405 which rationalize the downward projection of the pycnocline in terms of large-scale, wind-
406 driven Ekman flows and, in some cases, the integrated effects of deep baroclinic eddies
407 (Wolfe & Cessi, 2010; Nikurashin & Vallis, 2012).

408 In conclusion, elevated stratification within the high-latitude Southern Ocean in-
409 ternal pycnocline is generated by winter-persistent sea ice melting, and descends into the
410 ocean interior at ACC fronts. Both of these elements are absent from current theoret-
411 ical perspectives on pycnocline formation, including those considering the Southern Ocean’s
412 role (Gnanadesikan, 1999; Karsten et al., 2002; Wolfe & Cessi, 2010; Nikurashin & Val-
413 lis, 2012; D. P. Marshall et al., 2017). Such Southern Ocean-focused theories imply that
414 the internal pycnocline’s depth is determined by an intricate interplay between wind forc-
415 ing, baroclinic eddies and surface buoyancy fluxes. However, they assume that the in-
416 ternal pycnocline’s stratification reflects the meridional density gradient at the surface
417 of the Southern Ocean, and that this gradient is shaped by annual-mean surface buoy-
418 ancy fluxes. Our work indicates that establishment of the internal pycnocline relies on
419 the maintenance of a strong vertical density gradient at the base of the winter mixed layer
420 in subpolar seas, enabled by the northward drift of Antarctic sea ice and the persistence
421 of net sea ice melt.

422 A pressing question emerging from this work concerns how the internal pycnocline
423 generation mechanism discussed here, which focuses on the Southern Ocean’s beta ocean
424 regime, connects to classical pycnocline theories applying to the alpha ocean regime equa-
425 torward of the Southern Ocean. The illustrations of the internal pycnocline’s structure
426 in Fig. 1 show that the pycnocline transitions smoothly across the alpha-beta ocean bound-
427 ary. This points to the existence of a link between global-ocean transport pathways (such
428 as the overturning circulation) and sea-ice ocean interactions in the Southern Ocean –
429 the nature of which is difficult to untangle from the available monthly-mean model out-
430 put considered in our study. One possibility is that the internal pycnocline is primar-

431 ily generated in the subpolar Southern Ocean as explained in this work, and that the pyc-
432 noclone’s high-PV sheets are then projected northward by e.g., mesoscale eddy stirring.
433 Another possibility is that the internal pycnocline in the alpha ocean regime to the north
434 of the Southern Ocean is generated as proposed by classical theories, and that there is
435 a long-timescale adjustment between the processes governing northern and Southern Ocean
436 pycnocline formations - such that a continuous internal pycnocline emerges across the
437 alpha-beta ocean transition.

438 The main caveat of this work is that much of the analysis is qualitative. The large
439 computational resources required for these model simulations limit our ability to run mul-
440 tiple sensitivity experiments, and to save the model output needed to perform a more
441 quantitative analysis. A further challenge to more quantitatively test the ideas put for-
442 ward here is the wide range of spatio-temporal scales of the processes pertinent to in-
443 ternal pycnocline formation. Such scales span from the subdaily timescales of the local-
444 ized turbulent processes implicated in entrainment to the centennial (and longer) timescales
445 of basin-wide adjustment equatorward of the Southern Ocean. Thus, elucidating the role
446 of ice-ocean interactions in the Southern Ocean in generating the internal pycnocline is
447 likely to require a dual approach that captures and connects such disparate scales. Process-
448 targeted observations and turbulence-resolving modelling of the evolution of Southern
449 Ocean stratification under ice will be required to unravel the key stratification-controlling
450 processes. In turn, a hierarchy of basin-scale, eddy-resolving models of varying degree
451 of idealisation will be needed to establish the mechanisms via which under-ice Southern
452 Ocean processes may influence, or be influenced by, the rest of the global ocean. While
453 these requirements pose major technological and computational difficulties, the recent
454 rapid changes exhibited by Southern Ocean sea ice (Eayrs et al., 2021) highlight the im-
455 portance of discerning the potential pycnocline-generating role of regional ice-ocean in-
456 teractions.

457 **Appendix A Model comparison with observations**

458 While the model is thoroughly validated elsewhere (Kiss et al., 2020), for the pur-
459 pose of this work we note that the model broadly reproduces the observed structure of
460 the internal pycnocline (cf. Figs. 1 and A1), with two modest differences. First, the sep-
461 aration between high-stratification sheets in the observations is more subtle than in the
462 model. This is at least in part due to observations, which represent a snapshot of the

ocean, also including finescale motions (e.g., internal waves) and measurement noise. It is also likely that the model exaggerates the inter-sheet gap in the ocean interior, as the model's limited resolution does not fully capture the (sub-)mesoscale re-stratification processes expected to moderate vertical gradients in interior stratification (Bachman & Klocker, 2020), and as the model includes no background vertical diffusivity. Second, the densities of the observed high-stratification sheets are slightly lighter (typically by 0.1 - 0.2 kg m⁻³) than those in the model.

Appendix B Stratification Control Index

A key theoretical concept in our analysis of the model simulation is the Stratification Control Index, SCI, which is considered here to assess the degree of spiciness in a stable stratification (Stewart & Haine, 2016). The SCI is defined as the ratio of the spice frequency, $K^2 = g(\alpha\partial_z\Theta + \beta\partial_zS_A)$, to the buoyancy frequency, $N^2 = g(\alpha\partial_z\Theta - \beta\partial_zS_A)$, where g is the gravitational acceleration, α is the thermal expansion coefficient, and β is the haline contraction coefficient (Ioc et al., 2010). Since planetary PV is proportional to the stratification, SCI can equally be interpreted to indicate the relative contributions of temperature and salinity to setting PV. By construction, the SCI has three distinct regimes: $\text{SCI} < -1$ corresponds to a stable stratification controlled by salinity where the thermal stratification is unstable (as often found in polar regions); $-1 < \text{SCI} < 1$ is associated with thermal and haline stratifications that are both stable; and $\text{SCI} > 1$ is obtained when temperature controls the density stratification in the presence of a destabilizing effect of salinity.

The SCI can be connected to several other stratification indicators more commonly used in the literature. The density ratio, $R_\sigma = (\alpha\partial_z\Theta)/(\beta\partial_zS_A)$, was first introduced by Turner (Turner, 1973) and can be related to the SCI as $R_\sigma = (\text{SCI} + 1)(\text{SCI} - 1)$. A difficulty with the density ratio is that it diverges when the salinity stratification vanishes, even in the presence of a stable thermal stratification. This is the reason why the SCI is preferred here. Subsequently, the Turner angle was also determined as the arc tangent of the ratio of spice to buoyancy frequencies (Ruddick, 1983). Hence, the SCI is simply the tangent of the Turner angle, uniquely defined for any stable stratification. Drawing on the properties of the Turner angle, salt fingering is implied to occur when $\text{SCI} > 1$, and diffusive convection develops when $\text{SCI} < -1$.

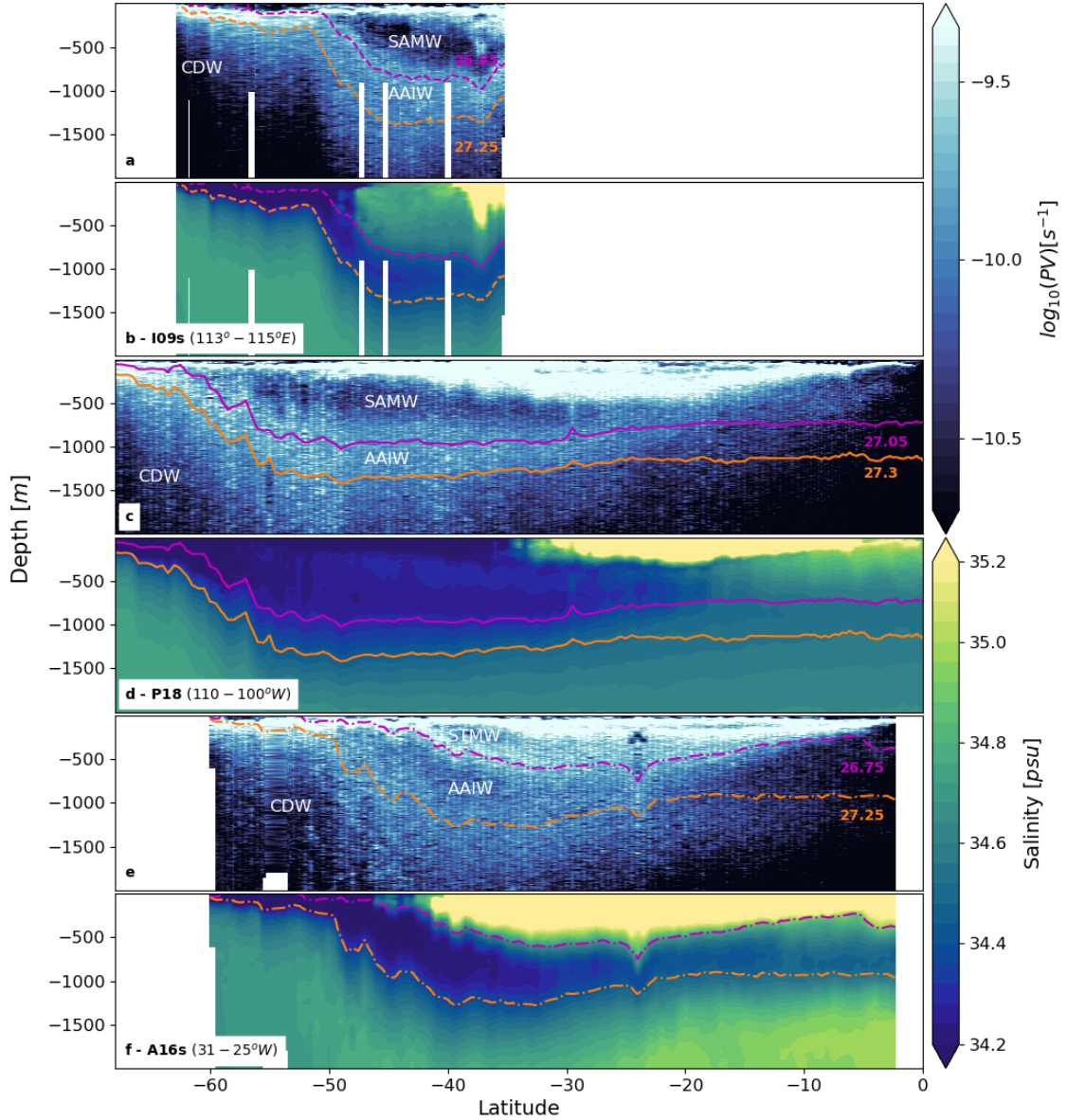


Figure A1. Potential vorticity and salinity from observations. Ship-based observations of (a,c,e) $\log_{10}(|PV|)$ and (b,d,f) salinity. (a,b) WOCE transect I09s from a R/V Aurora Australis cruise in January-February 2012, (c,d) WOCE transect P18 from a R/V Ronald H. Brown cruise in November 2016 - February 2017, and (e,f) WOCE transect A16s from R/V Ronald H. Brown cruise in January-February 2005. Colored lines are isopycnal surfaces approximately associated with the upper (magenta) and lower (orange) high-PV sheets, which together form the internal pycnocline

- . Subtropical Mode Water (STMW), Subantarctic Mode Water (SAMW), Antarctic Intermediate Water (AAIW), and Circumpolar Deep Water (CDW) are labeled.

Appendix C Thermal and haline surface buoyancy fluxes

The surface buoyancy flux, B , depends on both surface heating and freshwater input, and can be expressed as (Cronin & Sprintall, 2001)

$$B = \underbrace{-\frac{g\alpha Q}{\rho c_p}}_{B_H} + \underbrace{g\beta F_w SSS}_{B_{FW}}, \quad (C1)$$

where B_H is the buoyancy flux due to heating and cooling, and B_{FW} is the buoyancy flux due to freshwater input or loss. Q is the surface heat flux, F_w the surface freshwater input, ρ the surface density, c_p the specific heat capacity of seawater, and SSS the sea surface salinity. Q has units of W m^{-2} , F_w has units of m s^{-1} , and B has units of $\text{m}^2 \text{s}^{-3}$. In the coupled sea ice-ocean model used here, surface ocean fluxes are due to (i) restoring toward observed SSS , (ii) heat and freshwater exchanges with the atmosphere deduced from bulk formulae and the JRA55-do v1.3 forcing data set, and (iii) freshwater fluxes resulting from the melting and freezing of sea ice. In winter (Fig. C1, showing a mean over July-September 2015), the surface buoyancy flux indicates that changes in upper-ocean buoyancy under sea ice are almost entirely due to freshwater fluxes induced by the melting and freezing of sea ice. North of the sea-ice edge, the surface buoyancy flux transitions to being largely dominated by surface heat fluxes.

Acknowledgments

The authors thank the Consortium for Ocean-Sea Ice Modeling in Australia (COSIMA; www.cosima.org.au) for making the ACCESS-OM2 suite of models available at github.com/COSIMA/access-om2. Model runs were undertaken with the assistance of resources from the National Computational Infrastructure (NCI), which is supported by the Australian Government. This research was supported under Australian Research Council's Special Research Initiative for Antarctic Gateway Partnership (Project ID SR140300001). This project received grant funding from the Australian Government as part of the Antarctic Science Collaboration Initiative program. The work was supported in part by the Centre for Southern Hemisphere Oceans Research, a partnership between CSIRO, the Qingdao National Laboratory for Marine Science and Technology, the University of New South Wales and the University of Tasmania and by the Australian Antarctic Program Partnership. All the data used in this work are publicly available. The model code is available at github.com/COSIMA/access-om2, and the model output can be accessed at

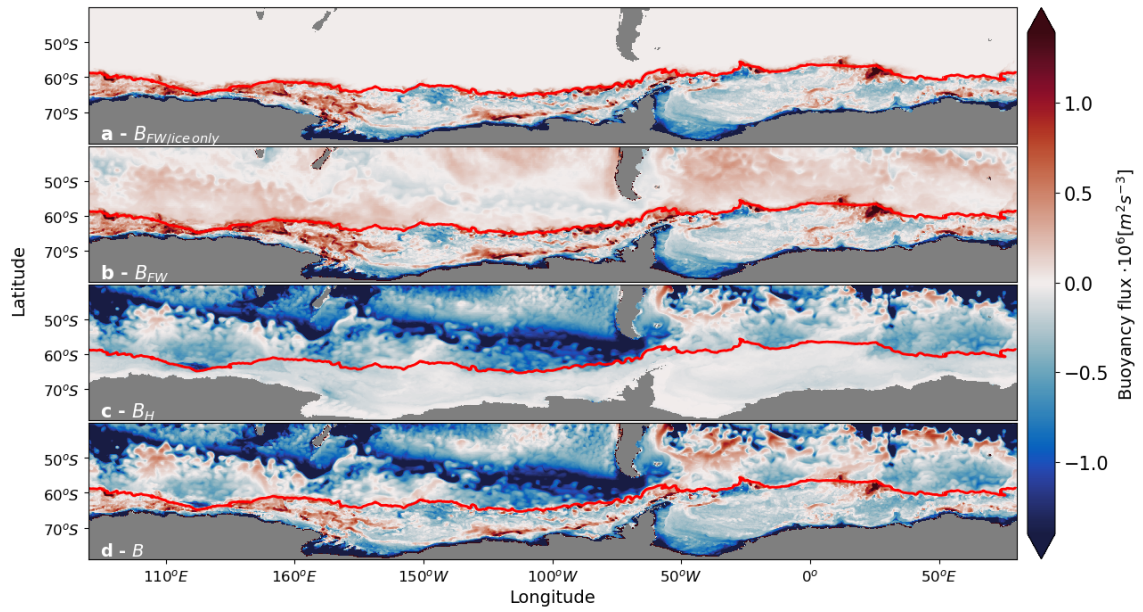


Figure C1. Surface buoyancy flux in the Southern Ocean. Wintertime (mean over July-September 2015) surface buoyancy flux due to (a) freshwater from sea-ice melting and freezing, (b) total surface freshwater input, and (c) surface heat flux. (d) Net surface buoyancy flux. Positive fluxes are directed into the ocean. The red line shows the sea-ice extent, defined as the northern terminus of sea-ice concentrations in excess of 15%.

524 <http://dx.doi.org/10.4225/41/5a2dc8543105a>. Observational transects can be downloaded
525 at <https://cchdo.ucsd.edu/cruise/09AR20120105> (WOCE transect I09s),
526 <https://cchdo.ucsd.edu/cruise/33RO20161119> (WOCE transect P18), and
527 <https://cchdo.ucsd.edu/cruise/33RO200501> (WOCE transect A16s).

528 References

- 529 Bachman, S., & Klocker, A. (2020). Interaction of jets and submesoscale dynam-
530 ics leads to rapid ocean ventilation. *Journal of Physical Oceanography*, *50*(10).
531 doi: 10.1175/JPO-D-20-0117.1
- 532 Bullister, J. L., Rhein, M., & Mauritzen, C. (2001). Deepwater Formation. In
533 G. Siedler, S. M. Griffies, J. Gould, & J. A. Church (Eds.), *Ocean circulation
534 and climate: a 21st century perspective* (pp. 227–253). Academic Press.
- 535 Carmack, E. C. (2007). The alpha/beta ocean distinction: A perspective on freshwa-
536 ter fluxes, convection, nutrients and productivity in high-latitude seas. *Deep-
537 Sea Research Part II: Topical Studies in Oceanography*, *54*(23-26), 2578–2598.
538 doi: 10.1016/j.dsr2.2007.08.018
- 539 Cronin, M., & Sprintall, J. (2001). Wind And Buoyancy-forced Upper Ocean. In *En-
540 cyclopedia of ocean sciences* (pp. 3219–3226). Elsevier. doi: 10.1006/rwos.2001
541 .0157
- 542 DeVries, T., & Holzer, M. (2019). Radiocarbon and Helium Isotope Constraints on
543 Deep Ocean Ventilation and Mantle-3He Sources. *Journal of Geophysical Re-
544 search: Oceans*, *124*(5), 3036–3057. doi: 10.1029/2018JC014716
- 545 DeVries, T., & Primeau, F. (2011). Dynamically and observationally constrained
546 estimates of water-mass distributions and ages in the global ocean. *Journal of
547 Physical Oceanography*, *41*(12), 2381–2401. doi: 10.1175/JPO-D-10-05011.1
- 548 DeVries, T., & Weber, T. (2017). The export and fate of organic matter in
549 the ocean: New constraints from combining satellite and oceanographic
550 tracer observations. *Global Biogeochemical Cycles*, *31*(3), 535–555. doi:
551 10.1002/2016GB005551
- 552 Eayrs, C., Li, X., Raphael, M. N., & Holland, D. M. (2021). Rapid decline
553 in Antarctic sea ice in recent years hints at future change. *Nature Geo-
554 science*, *14*(7), 460–464. Retrieved from [http://dx.doi.org/10.1038/
555 s41561-021-00768-3](http://dx.doi.org/10.1038/s41561-021-00768-3) doi: 10.1038/s41561-021-00768-3

- 556 Evans, D. G., Zika, J. D., Naveira Garabato, A. C., & Nurser, A. J. (2018). The
 557 Cold Transit of Southern Ocean Upwelling. *Geophysical Research Letters*,
 558 *45*(24), 13,386–13,395. doi: 10.1029/2018GL079986
- 559 Gnanadesikan, A. (1999, mar). A Simple Predictive Model for the Structure of the
 560 Oceanic Pycnocline. *Science*, *283*(5410), 2077–2079. doi: 10.1126/science.283
 561 .5410.2077
- 562 Haumann, F. A., Gruber, N., Münnich, M., Frenger, I., & Kern, S. (2016). Sea-
 563 ice transport driving Southern Ocean salinity and its recent trends. *Nature*,
 564 *537*(7618), 89–92. doi: 10.1038/nature19101
- 565 Huang, R. X. (1988, apr). On Boundary Value Problems of the Ideal-Fluid Thermo-
 566 cline. *Journal of Physical Oceanography*, *18*(4), 619–641. doi: 10.1175/1520
 567 -0485(1988)018<0619:OBVPOT>2.0.CO;2
- 568 Ioc, Scor, & Iapso. (2010). The international thermodynamic equation of seawater
 569 – 2010: Calculation and use of thermodynamic properties. *Intergovernmental*
 570 *Oceanographic Commission, Manuals and Guides No. 56*(June), 196.
- 571 Karsten, R., Jones, H., & Marshall, J. (2002). The role of eddy transfer in setting
 572 the stratification and transport of a circumpolar current. *Journal of Physical*
 573 *Oceanography*, *32*(1), 39–54. doi: 10.1175/1520-0485(2002)032<0039:TROETI>2
 574 .0.CO;2
- 575 Khatiwala, S., Primeau, F., & Holzer, M. (2012). Ventilation of the deep ocean con-
 576 strained with tracer observations and implications for radiocarbon estimates
 577 of ideal mean age. *Earth and Planetary Science Letters*, *325-326*, 116–125.
 578 Retrieved from <http://dx.doi.org/10.1016/j.epsl.2012.01.038> doi:
 579 10.1016/j.epsl.2012.01.038
- 580 Kiss, A., McC Hogg, A., Hannah, N., Boeira Dias, F., B Brassington, G., Cham-
 581 berlain, M., ... Zhang, X. (2020). ACCESS-OM2 v1.0: A global ocean-sea
 582 ice model at three resolutions. *Geoscientific Model Development*, *13*(2). doi:
 583 10.5194/gmd-13-401-2020
- 584 Klocker, A. (2018). Opening the window to the Southern Ocean: The role of jet dy-
 585 namics. *Science Advances*, *4*(10). doi: 10.1126/sciadv.aao4719
- 586 Large, W. G., McWilliams, J. C., & Doney, S. C. (1994). Oceanic vertical mixing: A
 587 review and a model with a nonlocal boundary layer parameterization. *Reviews*
 588 *of Geophysics*, *32*(4), 363–403. doi: 10.1029/94RG01872

- 589 Lecomte, O., Goosse, H., Fichefet, T., De Lavergne, C., Barthélemy, A., & Zunz,
590 V. (2017). Vertical ocean heat redistribution sustaining sea-ice con-
591 centration trends in the Ross Sea. *Nature Communications*, 8(1). doi:
592 10.1038/s41467-017-00347-4
- 593 Libera, S., Hobbs, W., Klocker, A., Meyer, A., & Matear, R. (2022). Ocean-sea
594 ice processes and their role on multi-month predictability of Antarctic sea ice.
595 *Geophysical Research Letters*, 1–10. doi: 10.1029/2021gl097047
- 596 Luyten, J. R., Pedlosky, J., & Stommel, H. (1983, feb). The Ventilated Thermo-
597 cline. *Journal of Physical Oceanography*, 13(2), 292–309. doi: 10.1175/1520
598 -0485(1983)013<0292:TVT>2.0.CO;2
- 599 Marshall, D. P., Ambaum, M. H., Maddison, J. R., Munday, D. R., & Novak,
600 L. (2017). Eddy saturation and frictional control of the Antarctic Cir-
601 cumpolar Current. *Geophysical Research Letters*, 44(1), 286–292. doi:
602 10.1002/2016GL071702
- 603 Marshall, J., Adcroft, A. J., Hill, C., Perelman, L., & Heisey, C. (1997). A finite-
604 volume, incompressible Navier–Stokes model for studies of the ocean on
605 parallel computers. *J. Geophys. Res.*, 102, 5753–5766.
- 606 Marshall, J., Olbers, D., Ross, H., & Wolf-Gladrow, D. (1993, mar). Poten-
607 tial Vorticity Constraints on the Dynamics and Hydrography of the South-
608 ern Ocean. *Journal of Physical Oceanography*, 23(3), 465–487. doi:
609 10.1175/1520-0485(1993)023<0465:PVCOTD>2.0.CO;2
- 610 Martinson, D. G. (1990). Evolution of the southern ocean winter mixed layer and
611 sea ice: Open ocean deepwater formation and ventilation. *Journal of Geophysi-
612 cal Research*, 95(C7), 11641. doi: 10.1029/jc095ic07p11641
- 613 McCartney, M. S. (1977). Subantarctic Mode Water. *Deep-Sea Research*, 24, 103–
614 119.
- 615 Naveira Garabato, A., Allen, J., Leach, H., Strass, V., Pollard, R., Garabato, A., &
616 Leach, H. (2001). Mesoscale subduction at the Antarctic Polar Front driven
617 by baroclinic instability. *Journal of Physical Oceanography*, 2087–2107. doi:
618 10.1175/1520-0485(2001)031<2087:MSATAP>2.0.CO;2
- 619 Naveira Garabato, A. C., Williams, A. P., & Bacon, S. (2014). The three-
620 dimensional overturning circulation of the Southern Ocean during the WOCE
621 era. *Progress in Oceanography*, 120, 41–78. doi: 10.1016/j.pocean.2013.07.018

- 622 Nikurashin, M., & Vallis, G. (2012). A theory of the interhemispheric meridional
 623 overturning circulation and associated stratification. *Journal of Physical*
 624 *Oceanography*, *42*(10), 1652–1667. doi: 10.1175/JPO-D-11-0189.1
- 625 Nycander, J., Hieronymus, M., & Roquet, F. (2015). The nonlinear equation of state
 626 of sea water and the global water mass distribution. *Geophysical Research Let-*
 627 *ters*, *42*(18), 7714–7721. doi: 10.1002/2015GL065525
- 628 Orsi, A. H., Whitworth, T., & Nowlin, W. D. (1995). On the meridional extent and
 629 fronts of the Antarctic Circumpolar Current. *Deep-Sea Research Part I*, *42*(5),
 630 641–673. doi: 10.1016/0967-0637(95)00021-W
- 631 Pellichero, V., Sallée, J.-B., Schmidtko, S., Roquet, F., & Charrassin, J.-B. (2017,
 632 feb). The ocean mixed layer under Southern Ocean sea-ice: Seasonal cycle and
 633 forcing. *Journal of Geophysical Research: Oceans*, *122*(2), 1608–1633. doi: 10
 634 .1002/2016JC011970
- 635 Polyakov, I. V., Pnyushkov, A. V., Alkire, M. B., Ashik, I. M., Baumann, T. M.,
 636 Carmack, E. C., ... Yulin, A. (2017). Greater role for Atlantic inflows on
 637 sea-ice loss in the Eurasian Basin of the Arctic Ocean. *Science*, *356*(6335),
 638 285–291. doi: 10.1126/science.aai8204
- 639 Robinson, A., & Stommel, H. (1959). The Oceanic Thermocline and the Associated
 640 Thermohaline Circulation. *Tellus*, *11*(3), 295–308. doi: 10.3402/tellusa.v11i3
 641 .9317
- 642 Roquet, F., Ferreira, D., Caneill, R., Schlesinger, D., & Madec, G. (2022).
 643 Unique thermal expansion properties of water key to the formation of
 644 sea ice on earth. *Science Advances*, *8*(46), eabq0793. Retrieved from
 645 <https://www.science.org/doi/abs/10.1126/sciadv.abq0793> doi:
 646 10.1126/sciadv.abq0793
- 647 Roquet, F., Madec, G., Brodeau, L., & Nycander, J. (2015). Defining a simplified
 648 yet "Realistic" equation of state for seawater. *Journal of Physical Oceanogra-*
 649 *phy*, *45*(10), 2564–2579. doi: 10.1175/JPO-D-15-0080.1
- 650 Ruddick, B. (1983). A practical indicator of the stability of the water column to
 651 double-diffusive activity. *Deep Sea Research Part A, Oceanographic Research*
 652 *Papers*, *30*(10), 1105–1107. doi: 10.1016/0198-0149(83)90063-8
- 653 Salmon, R. (1990, aug). The thermocline as an "internal boundary layer". *Journal*
 654 *of Marine Research*, *48*(3), 437–469. doi: 10.1357/002224090784984650

- 655 Samelson, R. M., & Vallis, G. K. (1997). Large-scale circulation with small diapyc-
 656 nal diffusion: The two-thermocline limit. *Journal of Marine Research*, *55*(2),
 657 223–275. doi: 10.1357/0022240973224382
- 658 Speer, K., & Forget, G. (2001). Global Distribution and Formation of Mode Wa-
 659 ters. In G. Siedler, S. M. Griffies, J. Gould, & J. A. Church (Eds.), *Ocean*
 660 *circulation and climate: a 21st century perspective* (pp. 211–226). Academic
 661 Press.
- 662 Stewart, K. D., & Haine, T. W. (2016). Thermobaricity in the transition zones be-
 663 tween alpha and beta oceans. *Journal of Physical Oceanography*, *46*(6), 1805–
 664 1821. doi: 10.1175/JPO-D-16-0017.1
- 665 Stommel, H., & Webster, J. (1962). Some properties of thermocline equations in a
 666 subtropical gyre. *Journal of Marine Research*, *20*(1), 42–56.
- 667 Sturm, M., & Massom, R. A. (2009). Snow and Sea Ice. In *Sea ice* (pp. 153–204).
 668 Oxford, UK: Wiley-Blackwell. doi: 10.1002/9781444317145.ch5
- 669 Talley, L. D. (2013). Closure of the global overturning circulation through the In-
 670 dian, Pacific, and southern oceans. *Oceanography*, *26*(1), 80–97. doi: 10.5670/
 671 oceanog.2013.07
- 672 Tamsitt, V., Drake, H. F., Morrison, A. K., Talley, L. D., Dufour, C. O., Gray,
 673 A. R., ... Weijer, W. (2017). Spiraling pathways of global deep waters to
 674 the surface of the Southern Ocean. *Nature Communications*, *8*(1), 1–10. doi:
 675 10.1038/s41467-017-00197-0
- 676 Thorndike, A. S., & Colony, R. (1982). Sea ice motion in response to geostrophic
 677 winds. *Journal of Geophysical Research*, *87*(C8), 5845. doi: 10.1029/
 678 jc087ic08p05845
- 679 Turner, J. S. (1973). *Buoyancy Effects in Fluids*. Cambridge University Press. doi:
 680 10.1017/CBO9780511608827
- 681 Vallis, G. K. (2006). *Atmospheric and Oceanic Fluid Dynamics*. Cambridge Univer-
 682 sity Press, Cambridge. doi: 10.1017/cbo9780511790447
- 683 Welander, P. (1959, aug). An Advective Model of the Ocean Thermocline. *Tellus*,
 684 *11*(3), 309–318. doi: 10.3402/tellusa.v11i3.9316
- 685 Wilson, E. A., Riser, S. C., Campbell, E. C., & Wong, A. P. (2019). Winter
 686 upper-ocean stability and ice-ocean feedbacks in the sea ice-covered South-
 687 ern Ocean. *Journal of Physical Oceanography*, *49*(4), 1099–1117. doi:

688 10.1175/JPO-D-18-0184.1

689 Wolfe, C. L., & Cessi, P. (2010). What sets the strength of the middepth stratifica-
690 tion and overturning circulation in eddying ocean models? *Journal of Physical*
691 *Oceanography*, *40*(7), 1520–1538. doi: 10.1175/2010JPO4393.1

692 Young, W. R., & Ierley, G. R. (1986, nov). Eastern Boundary Conditions and Weak
693 Solutions of the Ideal Thermocline Equations. *Journal of Physical Oceanogra-*
694 *phy*, *16*(11), 1884–1900. doi: 10.1175/1520-0485(1986)016<1884:EBCAWS>2.0
695 .CO;2